Problem Session

2022. 12.10.

Aoi Takeuchi

A synthetic scheme for peptidic natural product **7** is described. Some stereochemistries are not shown for **4**, **7** and **9**. Please read the **Note** in the next page and provide a reaction mechanism of each step, the structures of **3** and **6**, and stereochemistries of **4**, **7** and **9**.

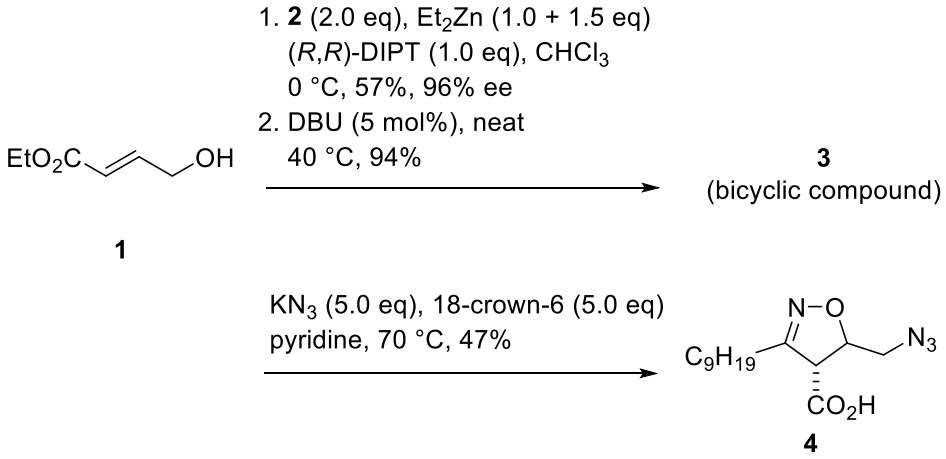

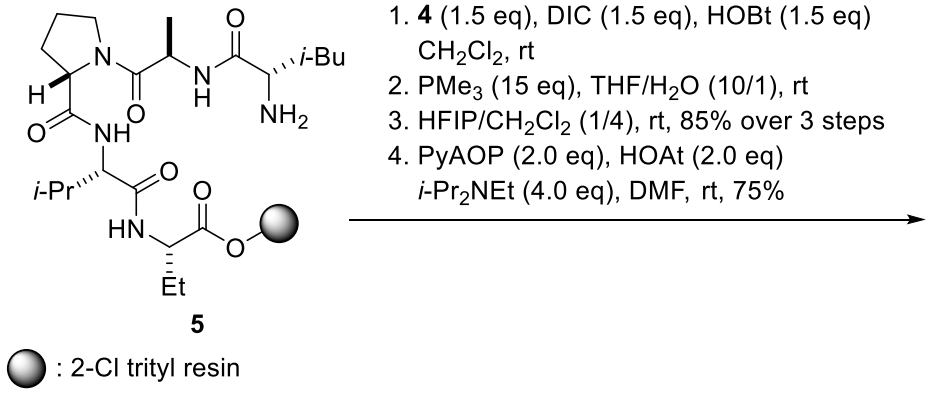

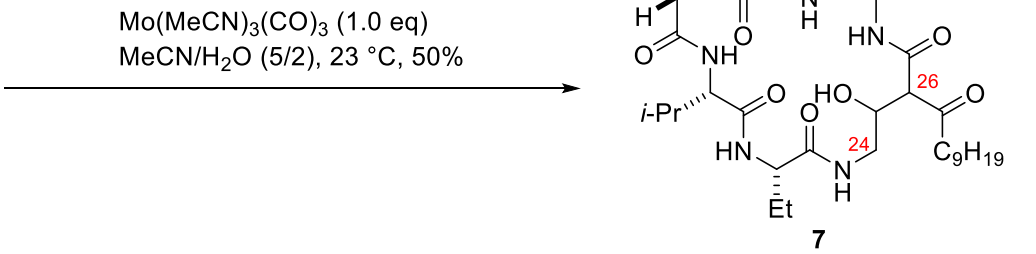

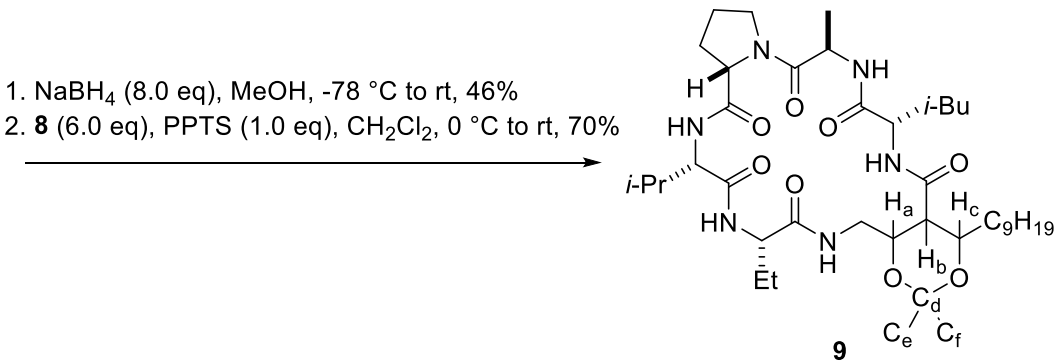

J-coupling	$^{13}C\{^{1}H\}$ chemical shifts
$J_{H_a\text{-}H_b}$ = 3.1 Hz	C_d: 98.1 ppm
$J_{H_b\text{-}H_c}$ = 3.1 Hz	$C_{e,f}$: 19.2, 29.5 ppm

Note

The reduction of **6** was investigated under two different conditions using ^{18}O-labelled water. As a result, ^{18}O-labelled isotopes **^{18}O-7** and **2^{18}O-7** were obtained with all the stereochemistries unchanged from the original **7** (see Table).

Table. Reaction conditions for reduction of **6** and composition of the products measured by LC-HRMS.

conditions for reduction of **6**	**7**:**^{18}O-7**:**2^{18}O-7**
Pd/C, H_2, AcOH, MeOH/$H_2{}^{18}O$ (5/1)	9:91:0
$Mo(MeCN)_3(CO)_3$, MeCN/ $H_2{}^{18}O$ (5/2)	0:20:80

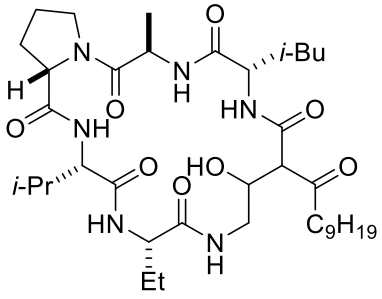

7

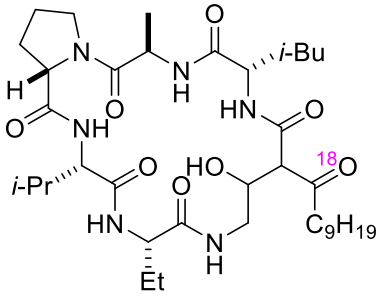

^{18}O-7

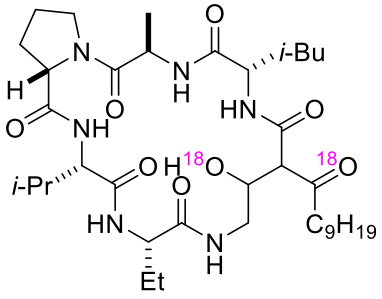

2^{18}O-7

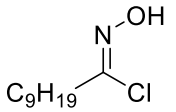

2

8

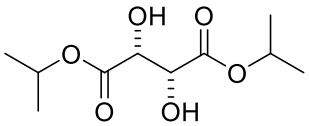

(*R*,*R*)-DIPT (diisopropyl tartrate)

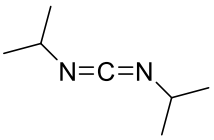

DIC
(diisopropylcarbodiimide)

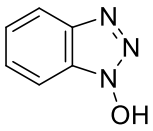

HOBt

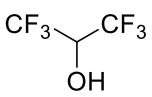

HFIP
(hexafluoroisopropanol)

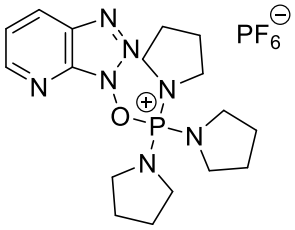

PyAOP

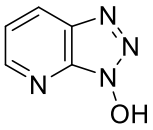

HOAt

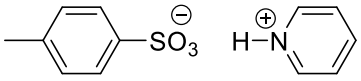

PPTS
(pyridinium *p*-toluenesulfonate)

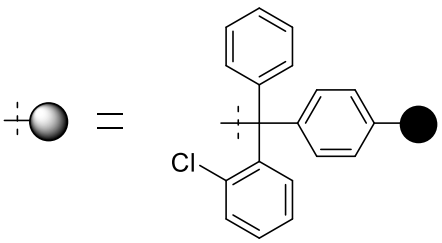

2-Cl trityl resin

Problem Session

2022. 12.10.

Aoi Takeuchi

Topic: Total synthesis and stereochemical determination of Mutanobactin D

Contents:

1. Mutanobactin D (**7**)

1.1. Mutanobactin D

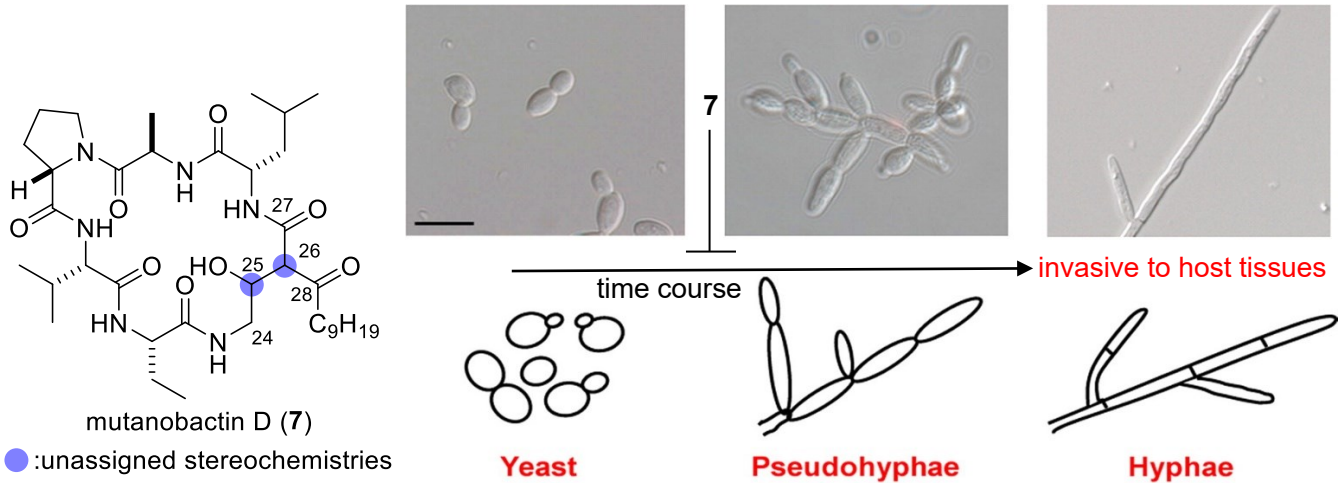

Figure 1. Mutanobactin D (**7**) and major morphologies of *Candida albicans* as visualized by differential interference contrast microscopy[1] (bar = 10 μm).

isolation:	from *Streptococcus mutans* by Cichewicz (2012) [2,3,4]
biological activities:	reduce yeast-to-hyphae transition of the pathogenic yeast *Candida albicans*[3]
	suppress biofilm formation of *Candida albicans* without growth inhibition[4]
stereochemistries:	C-25 and C-26 were not assigned[4].
total synthesis:	Carreira[5] (2021, stereochemical determination)

1.2. Potentially labile β-hydroxy-β′-keto-γ-amino amide subunit

The β-hydroxy-β′-keto-γ-amino amide subunit possibly undergo several reactions at C-26 flanked by two carbonyls. Accordingly, the configurations of C-25 and C-26 are potentially subject to isomerization (Figure 2).

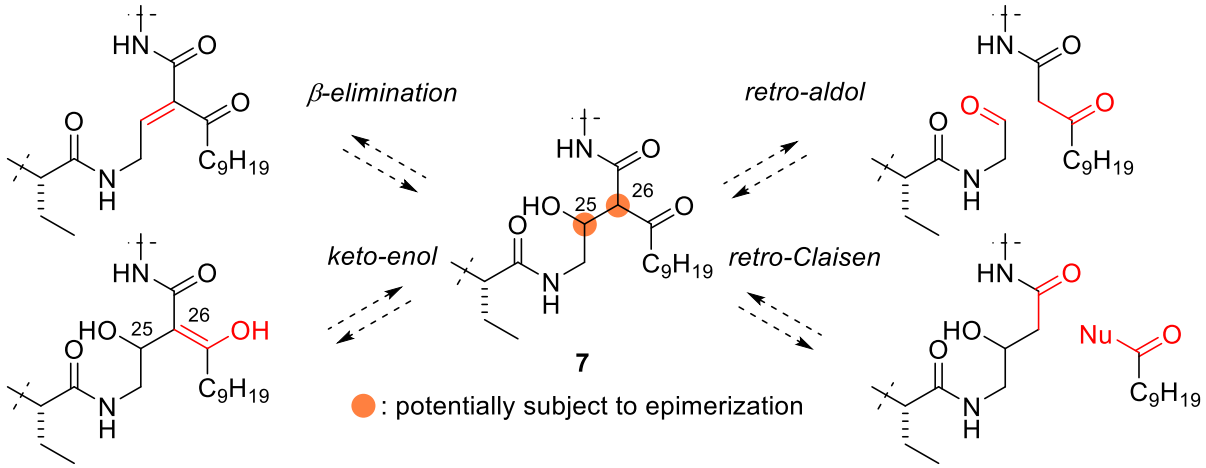

Figure 2. Potential reactivity of β-hydroxy-β′-keto-γ-amino amide subunit.

Conveniently, H-26 of **7** did not undergo H-D exchange in DMSO-d_6/D_2O (5/1) with 5% TFA-*d*, suggesting **7** itself is unlikely to undergo configurational scrambling at C-26[5]. Yet, similar cautions have to be paid during the synthesis of **7** because intermediates bearing β-hydroxy-β′-keto-γ-amino amides share the same concerns.

2. Synthesis of azido carboxylic acid **4**

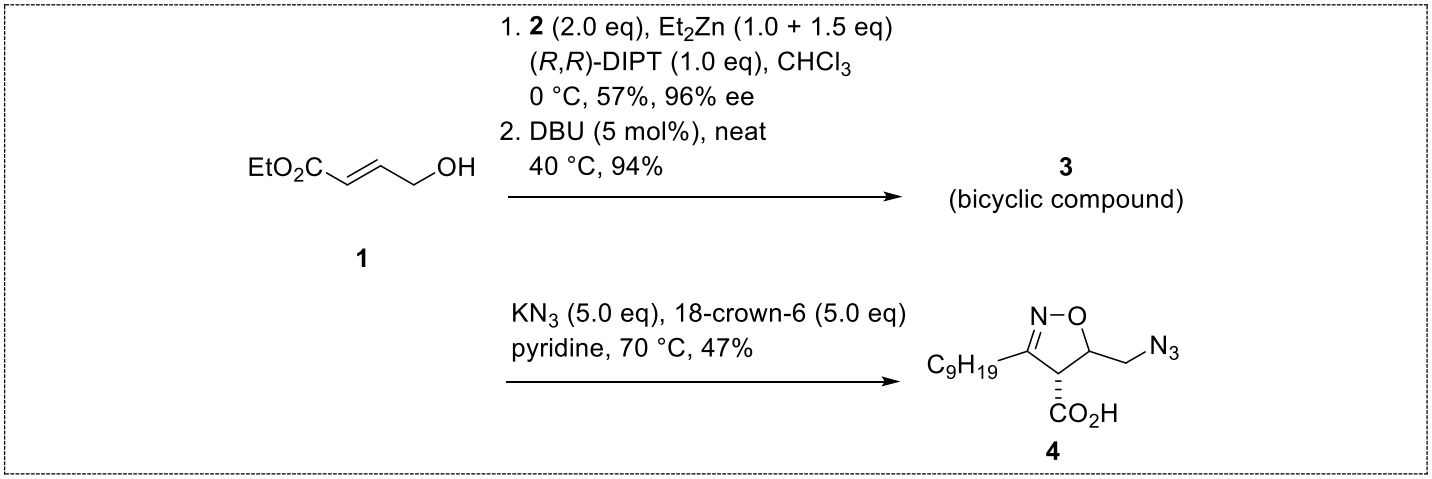

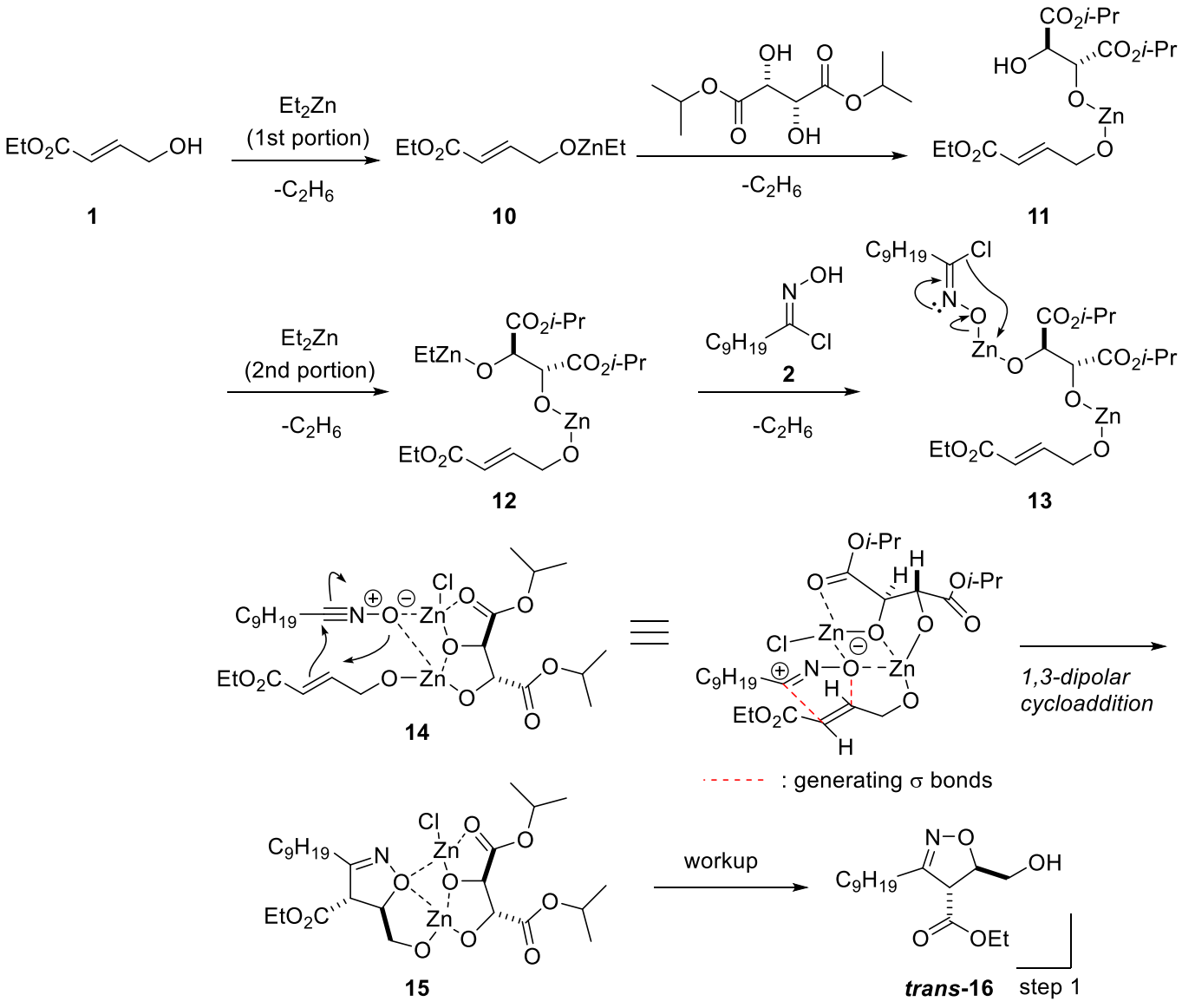

The enantioselectivity of 1,3-dipolar cycloaddition[6] could be explained by bimetallic transition state model[7], in which the rigid *cis*-5/5-fused bicyclic structure is formed by zinc-bridging.

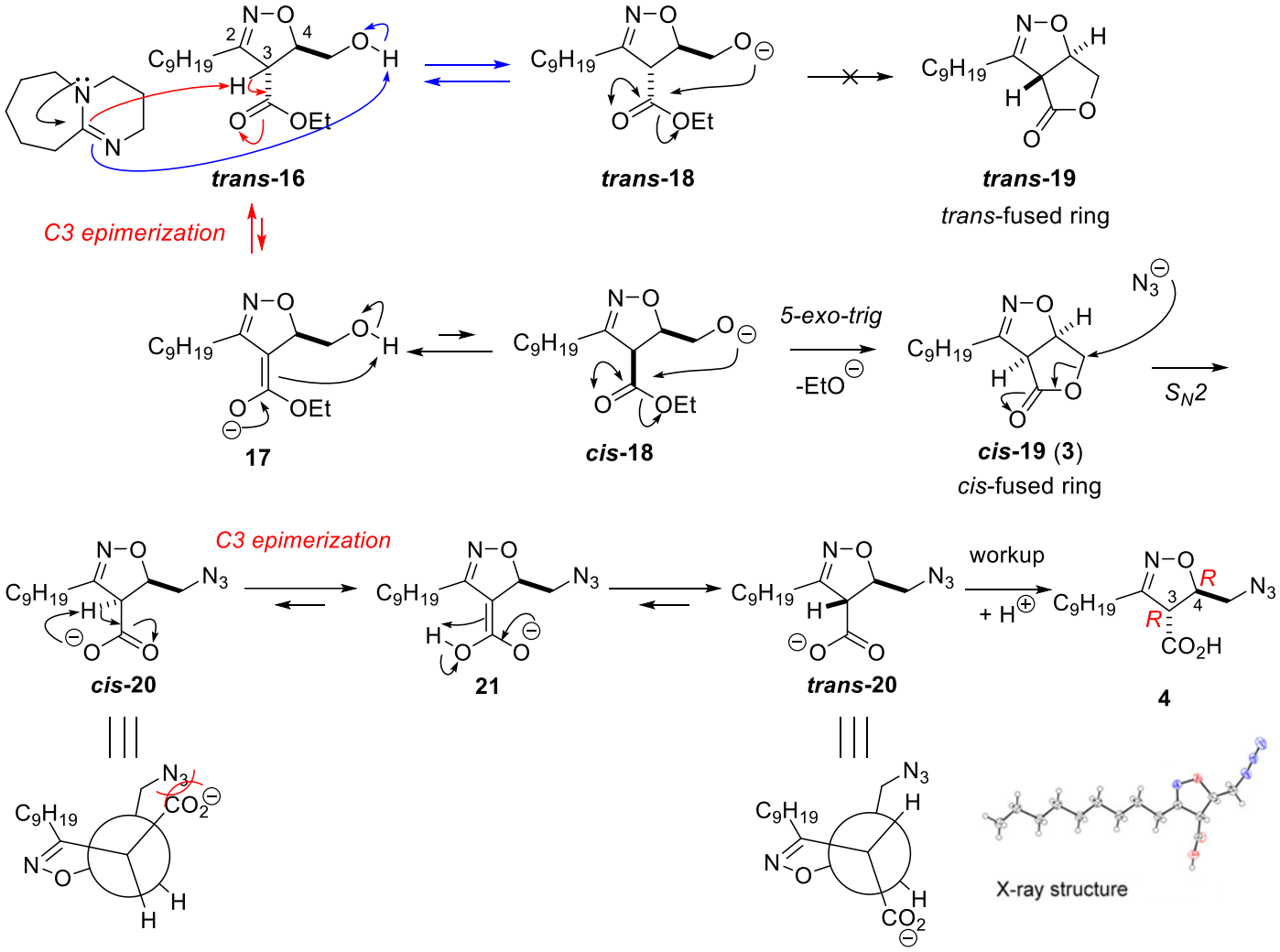

3. Configurational assignment of Mutanobactin D

3.1. Karplus equation[8,9]

Firstly described in 1959, the vicinal spin-spin coupling constant $^3J_{H\text{-}H}$ theoretically correlates with the dihedral angle θ (H-C-C-H) following Karplus equation (eq. 1), originally derived from Valence Bond calculations.

$$^3J_{H\text{-}H} = A\cos^2\theta + B\cos\theta + C \qquad \text{(eq. 1)}$$

The values of the Karplus coefficients, *A*, *B*, and *C*, are parameterized depending on particular molecule types, and atoms [ex. A = 7.76, B = -1.1, C = 1.4 for $^3J_{H\text{-}H}$ (H-Csp^3-Csp^3-H), A = 6.98, B = -1.38, C = 1.72 for $^3J_{H\text{-}H}$ (H-N-Csp^3-H)][10,11]. Based on this equation, $^3J_{H\text{-}H}$ is small when one H is *gauche* to another H (θ = 60°), and large when one H is *anti-periplanar* to another H (θ = 180°) (Figure 3).

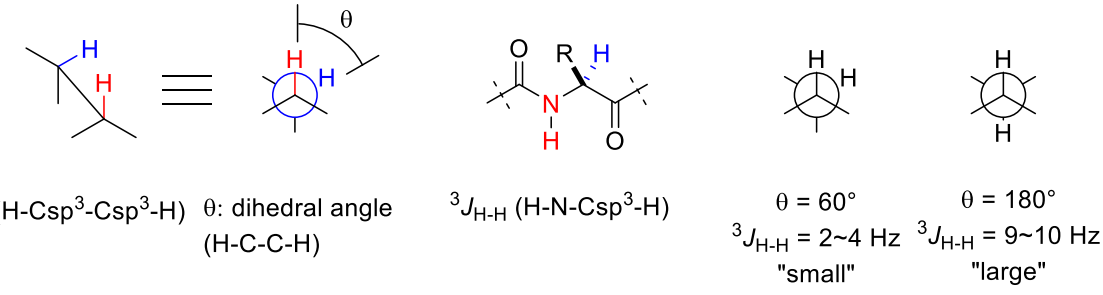

Figure 3. Dihedral angle and its dependence of vicinal spin-spin coupling constants.

The dihedral angle dependence of the magnitude of vicinal couplings results from molecular orbital overlap. Since the σ C-C bond and the σ C-H bonds are nearly perpendicular, so these two bonds have little overlap. Overlap of the σ C-H bond orbitals governs the magnitude of the coupling.

- Maximum orbital overlap occurs when the dihedral angle is 0° and 180° (→ large $^3J_{H\text{-}H}$)
- The orbital overlap is minimal when the dihedral angle is 90° (→ small $^3J_{H\text{-}H}$)

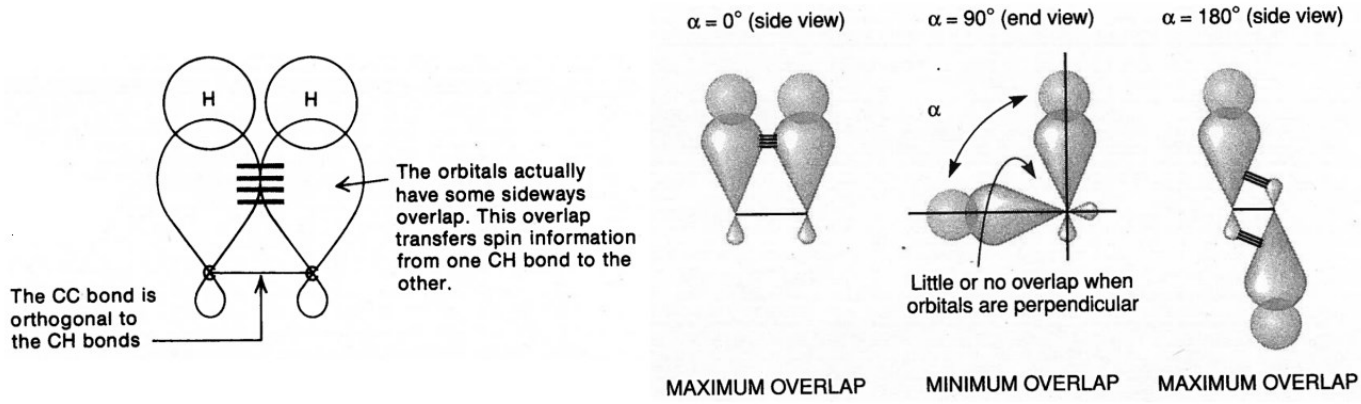

Figure 4. Schematic relationship between vicinal spin-spin coupling constants and molecular orbital overlap.

3.2. Haasnoot-Altona equation

While theoretically defined Karplus equation is approximately in accord with experimental data, dependences on substituents attached to the H-C-C-H, and on bond angle and length were not considered in the equation, although the latter two molecular properties have proved to have minor effects[12]. Actually, electronegativity and relative positions of substituents has secondary impact in determining the magnitude of vicinal coupling constants, next to dihedral angle[13]. Thus, refined equation considering substituent electronegativity orientation was proposed by Haasnoot and Altona in 1980[10,14] (eq 2). Each parameter was determined by fitting a curve to experimental coupling constants.

$$^3J = 14.64\cos^2\theta - 0.78\cos\theta + 0.58 + \Sigma\lambda_i\,[0.34 - 2.31\cos^2(\xi_i\,\theta + 16.9\,|\lambda_i|)] \qquad \text{(eq. 2)}$$

where λ_i is empirical parameters accounting for the electronegativity of the substituents and ε_i stands for orientation of the substituents (ξ_i = +1 for S_1 and S_3 and ξ_i = -1 for S_2 and S_4, Figure 5a). For a case study, $^3J_{Ha\text{-}Hb}$ of **9** was calculated based on eq. 1 and eq. 2 (Figure 5b). Substituent electronegativity orientation influences the coupling in two ways; they cause a change in overall magnitude of the Karplus equation, and they cause a shift of the maxima and minima of the curve (Figure 6, Table 1)[15].

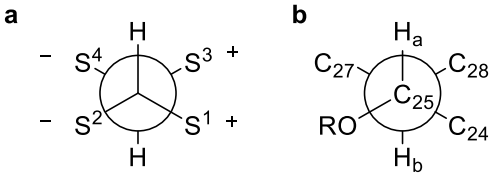

coefficients for the Haasnoot equation[16].

substituents	ξ_i	λ_i
C24	+1	0.68
C27	-1	0.42
C28	+1	0.62
OR	-1	1.40

Figure 5. (a) Definition of positive and negative orientations of substituents S^1-S^4 with respect to the vicinally coupled protons in tetrasubstituted ethane. (b) Newman projection of C_{25}-C_{26} bond of **9**.

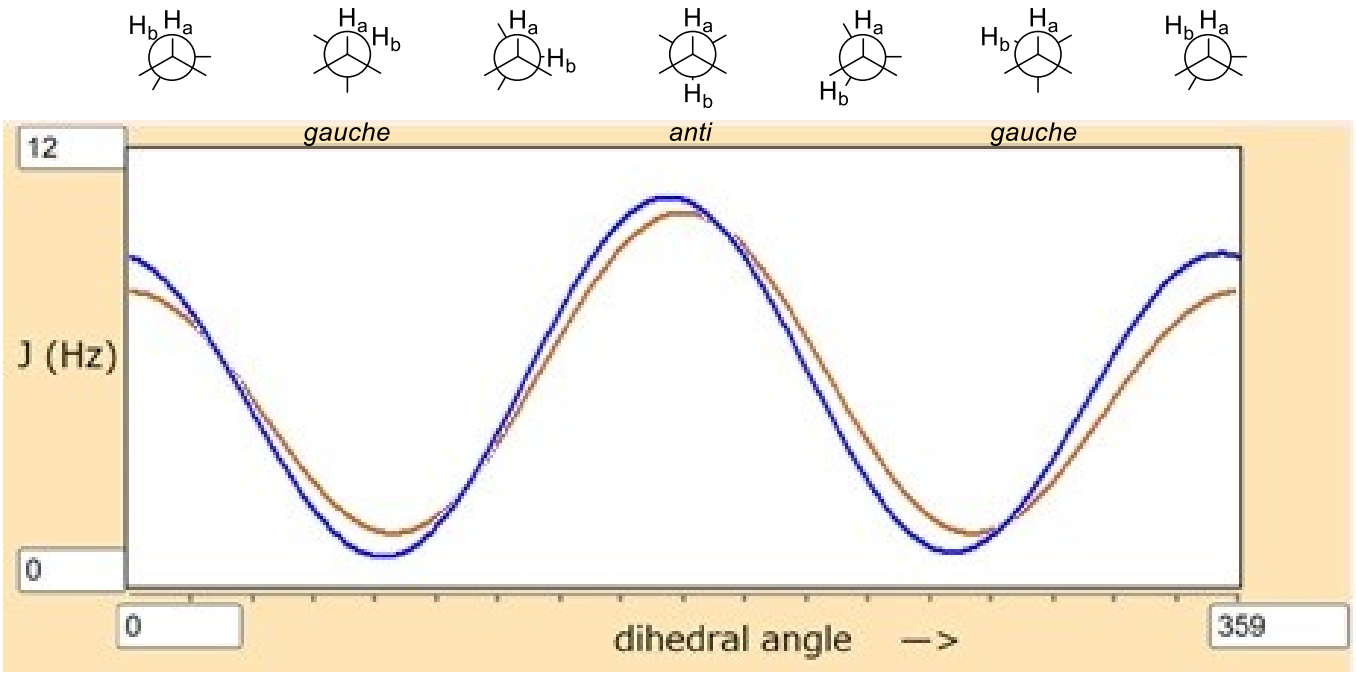

Figure 6. Calculated spin-spin coupling constants $^{3}J_{H_a\text{-}H_b}$ based on Karplus equation (orange) or Haasnoot equation (blue)[17].

Table 1. Calculated vicinal spin-spin coupling constant $^{3}J_{Ha\text{-}Hb}$

dihedral angle	θ = 60° *gauche*	θ = 180° *anti-periplanar*	θ = 300° *gauche*
Karplus equation	2.79	10.26	2.79
Haasnoot-Altona equation	2.05	10.61	3.41

Of note, it is possible to assign the relative configuration of acyclic systems by *J*-based configuration analysis integrating $^{3}J_{C\text{-}H}$ and $^{2}J_{C\text{-}H}$ other than $^{3}J_{H\text{-}H}$. (For details, see PS_140705_Takuya_Kaji)

3.3. Rychnovsky's correlation

The ^{13}C acetonide method developed by Rychnovsky[18,19], provided a valuable empirical method to assign the relative configurations of *syn*- and *anti*-1,3-diols. Diols are derivatized to the corresponding acetonides, and ^{13}C chemical shifts of the geminal methyl groups can be used to differentiate the two diastereomers. *Syn*-1,3-diol acetonides adopt chair conformations with differential axial and equatorial methyl groups. On the other hand, *anti*-1,3-diol acetonides prefer the twist-boat conformation to avoid 1,3-diaxial interactions with a methyl group and an either substituent (R^1 or R^3), resulting almost equivalent methyl groups. The chemical shift of the acetonide quaternary carbon is also diagnostic for configuration (Figure 7). As the size difference of substituents increase, the 1,3-dioxane ring tends to adopt a chair conformation[20,21,22].

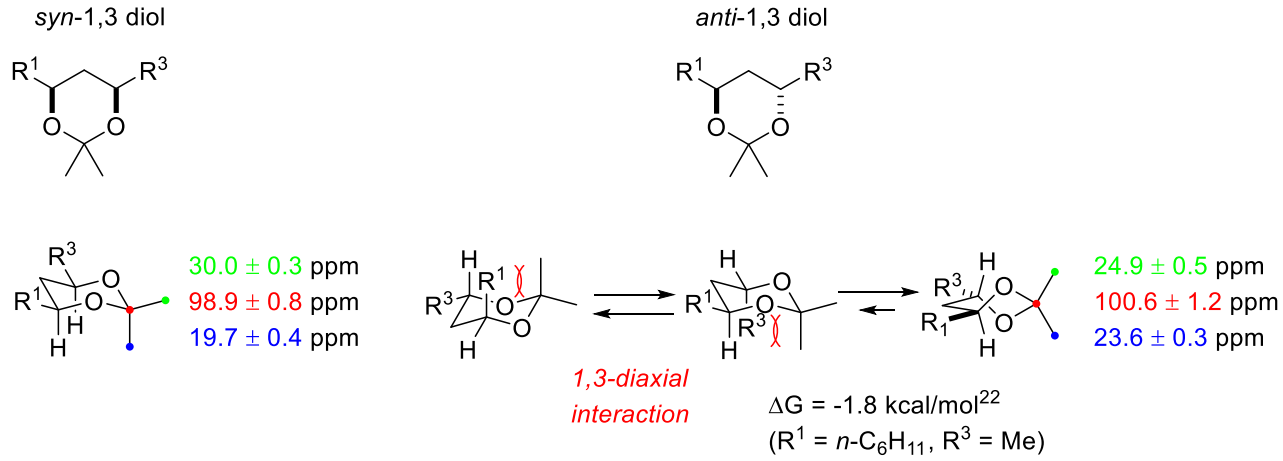

Figure 7. Conformation and typical $^{13}C\{^{1}H\}$ NMR chemical shifts of generic 1,3-diol acetonides.

3.4. Configurational assignment of acetonide **9** and mutanobactin D (**7**)

First, C25 of **9** is assigned as *R*-configuration tentatively according to the assumption that the (*R*)-C4 configuration of **4** is retained during the conversion to **9**. The ^{13}C NMR resonances for the acetonide methyls and ketal carbon strongly indicated a chair-like conformation for **9** and thereby the *syn*-1,3-diol acetonides in accordance with Rychnovsky's correlation (Figure 8).

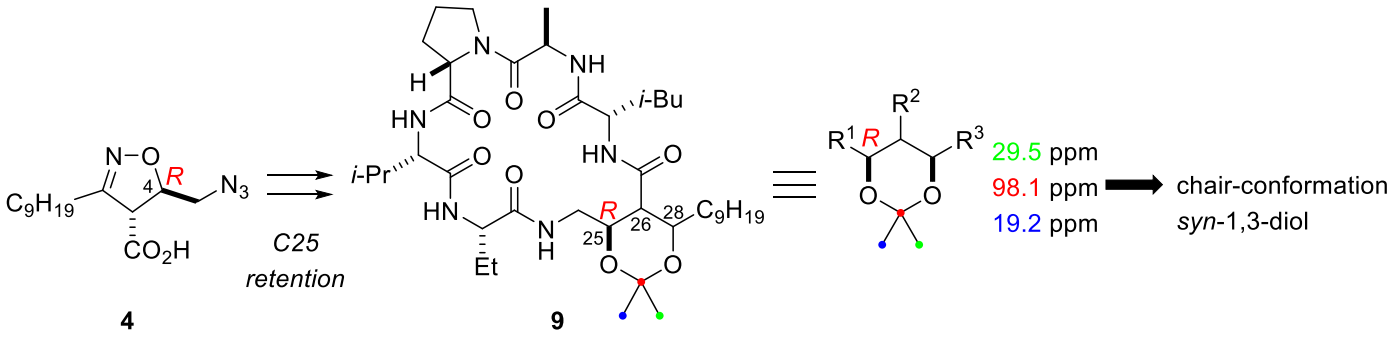

Figure 8. Configurational assignment of **9** based on Rychnovsky's correlation.

In this case, two configurations are possible depending on the configuration of C26. For (*R*)-C26, H_b is *anti-periplanar* to H_a and H_c (candidate A). Alternatively, for (*S*)-C26, H_b is *gauche* to H_a and H_c (candidate B). In the first case, $^3J_{H_a\text{-}H_b}$ and $^3J_{H_b\text{-}H_c}$ would be expected to correspond to 9–10 Hz and in the second case 2–4 Hz. The observed $^3J_{H_a\text{-}H_b} = {}^3J_{H_b\text{-}H_c} = 3.1$ Hz is consistent with candidate B and the assignment of C-26 as (*S*) in **9** (Figure 9).

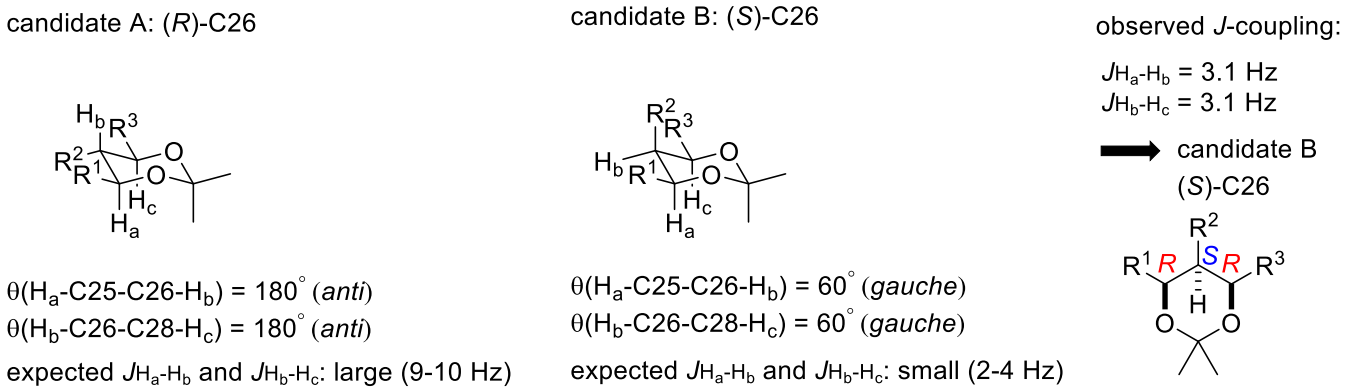

Figure 9. Configurational assignment of **9** based on *J*-coupling analysis.

Finally, it is necessary to validate the first assumption for the retained *R*-configuration of **9**. It was established that the configuration of *trans*-substituted isoxazoline in **6** is unchanged through the sequence based on the observation of a strong NOE between H24 and H26. Then, it is necessary to examine whether the configuration of C25 retains over the course of the isoxazoline ring-opening reaction (**6**→**7**). Related to this issue, it is considerable that the assigned configuration of **9** means that C26 undergoes epimerization during the isoxazoline cleavage and hydrolysis (Figure 10). Note that *R*/*S* assignment of the configuration of C26 inverses at the conversions from **6** to **7** and from **7** to **9** because of changing priorities of CIP designation (the configuration of C26 was distinguished by red/blue colors for help).

Isotopic labelling experiment in the **Note** would be of help to address these issues. The reduction with Pd/C afforded single-^{18}O-incorporated **^{18}O-7** (condition A), while the use of $Mo(MeCN)_3(CO)_3$ led to double-^{18}O-incorporated **2^{18}O-7** as a major product with a minor portion of **^{18}O-7** (condition B). This suggests the C26

epimerization proceeded in different mechanisms (Figure 11). The C26 epimerization possibly occurred via keto-enol tautomerization to give **^{18}O-7** in condition A, and via β-elimination[23] and re-addition of water to give **2^{18}O-7** in condition B. Since **^{18}O-7** and **2^{18}O-7** have the same configuration, it is concluded that the exchange of the hydroxy group of **21** occurred with retention of configuration at C25 in condition B. Collectively, these findings excluded configurational scrambling of C25 during N–O reduction and imine hydrolysis, and the assignment of the configuration of C25 as (*R*) in **9** was validated.

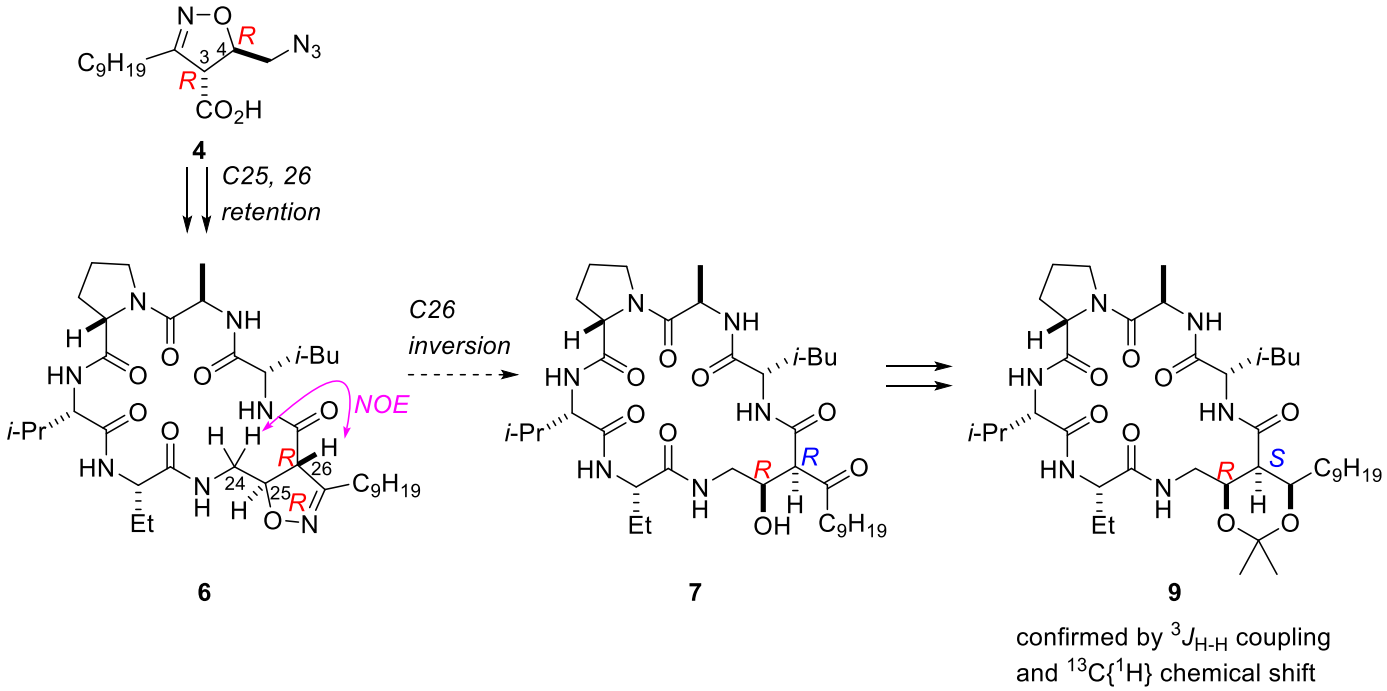

Figure 10. Assigned configurations of **6**, **7** and **9**.

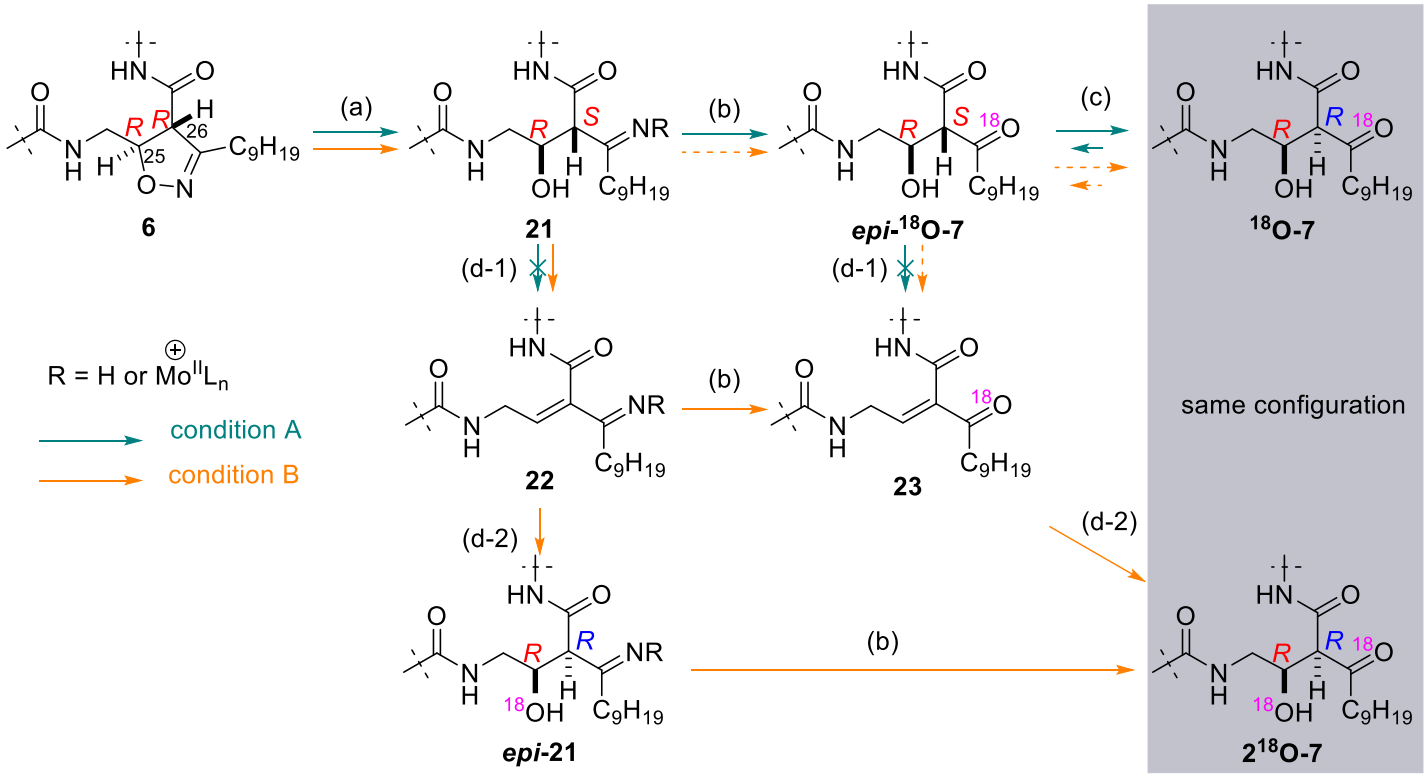

Figure 11. Possible pathways of the isoxazoline ring-opening reactions. Condition A: Pd/C, H_2, AcOH, MeOH/$H_2{}^{18}O$ (5/1), condition B: $Mo(MeCN)_3(CO)_3$, MeCN/$H_2{}^{18}O$ (5/2). (a) N–O reduction, (b) imine hydrolysis, (c) keto-enol tautomerization, (d-1) β-elimination, (d-2) re-addition of water.

3.5. Reaction mechanisms

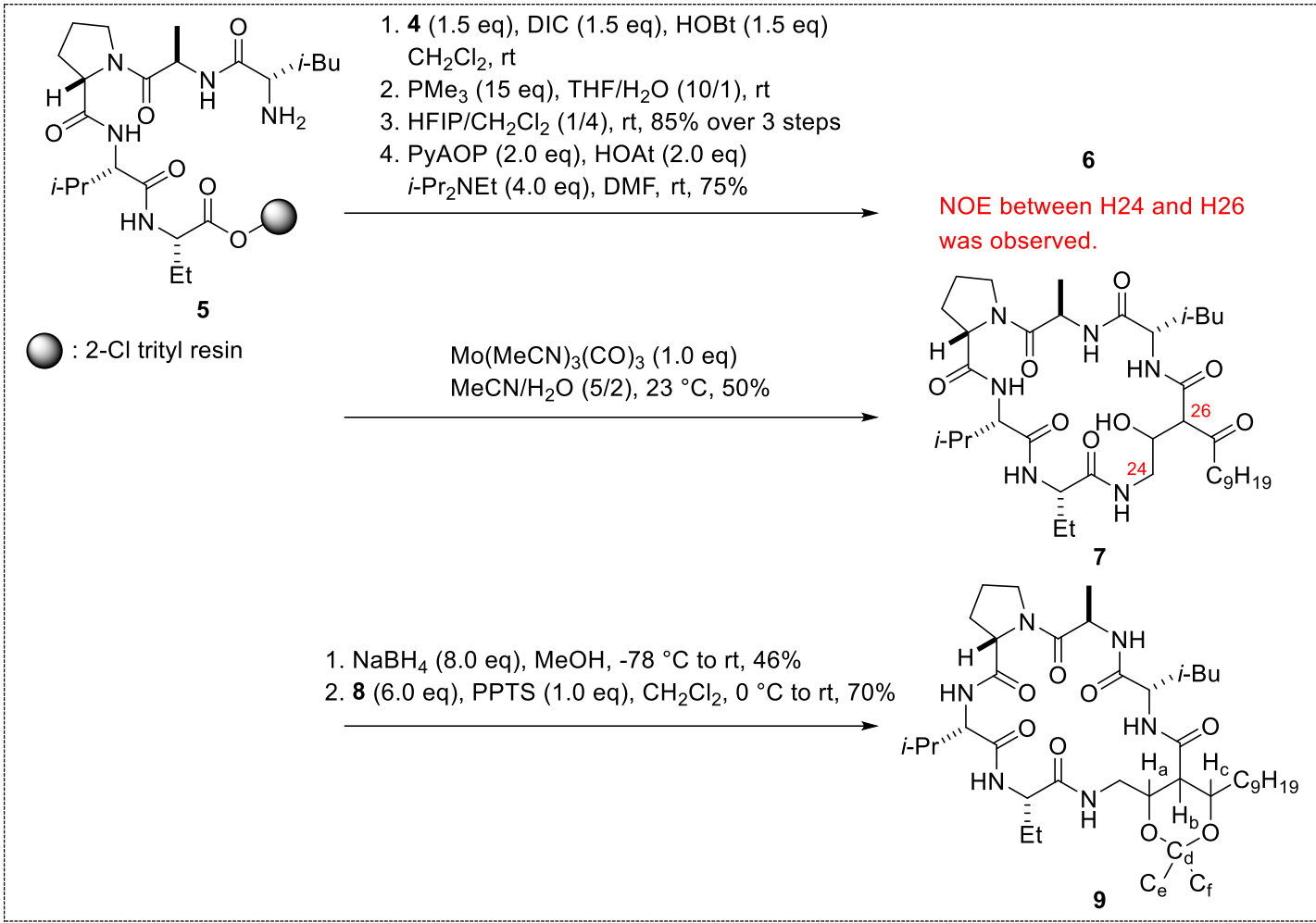

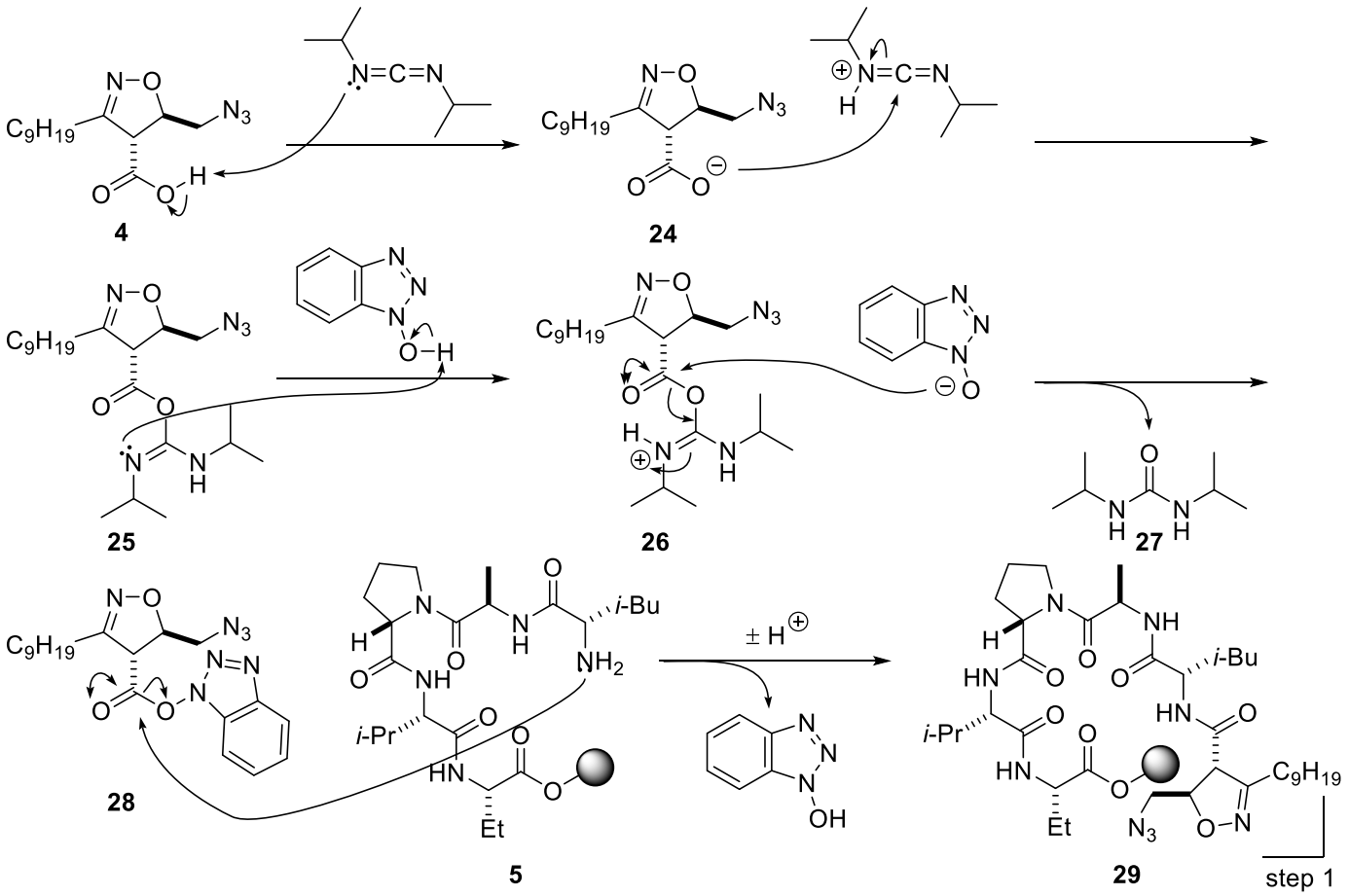

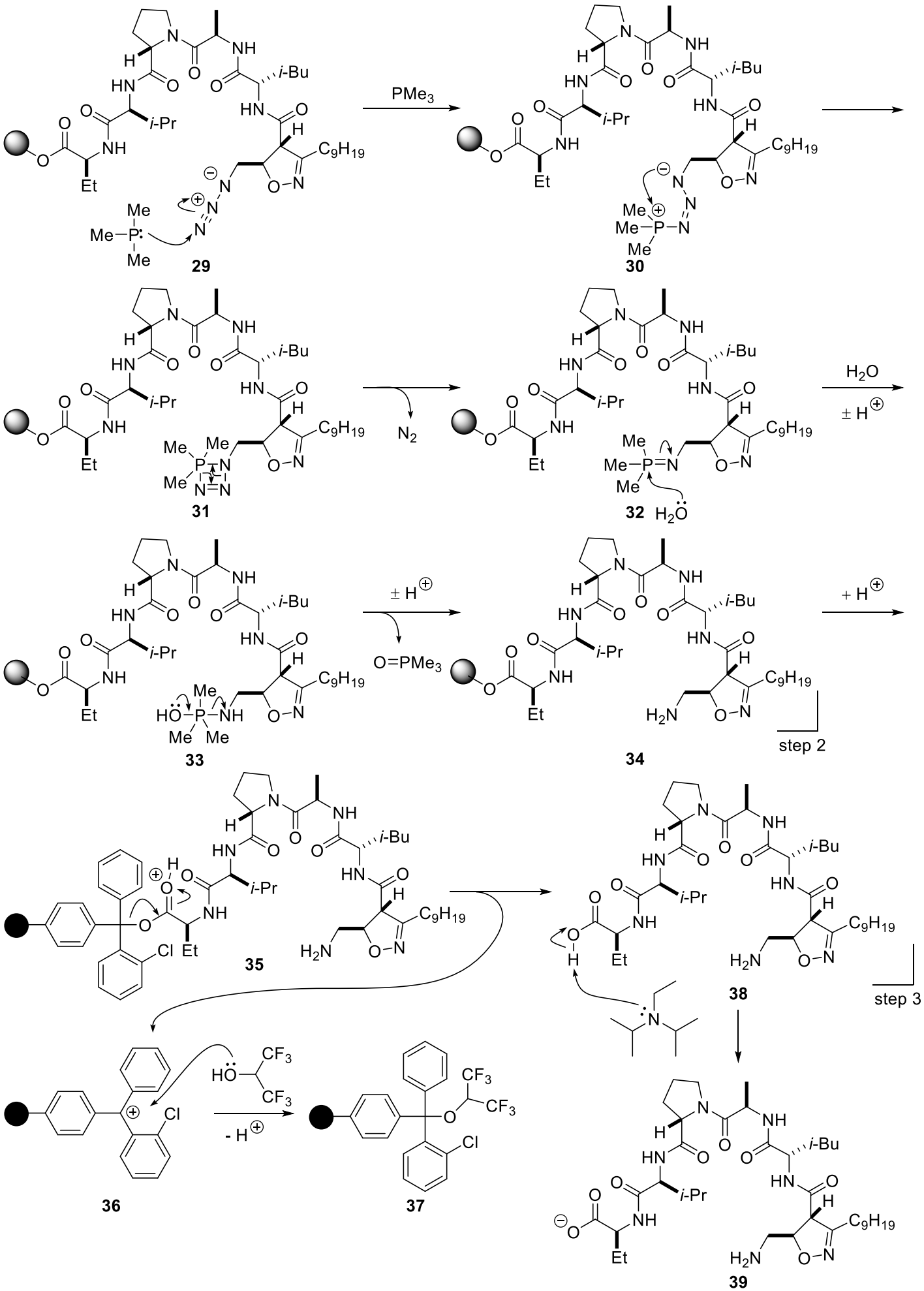
PMe3
29
30
31
N2
32
H2O
± H⊕
33
O=PMe3
34
+ H⊕
step 2
35
38
step 3
36
37
- H⊕
39

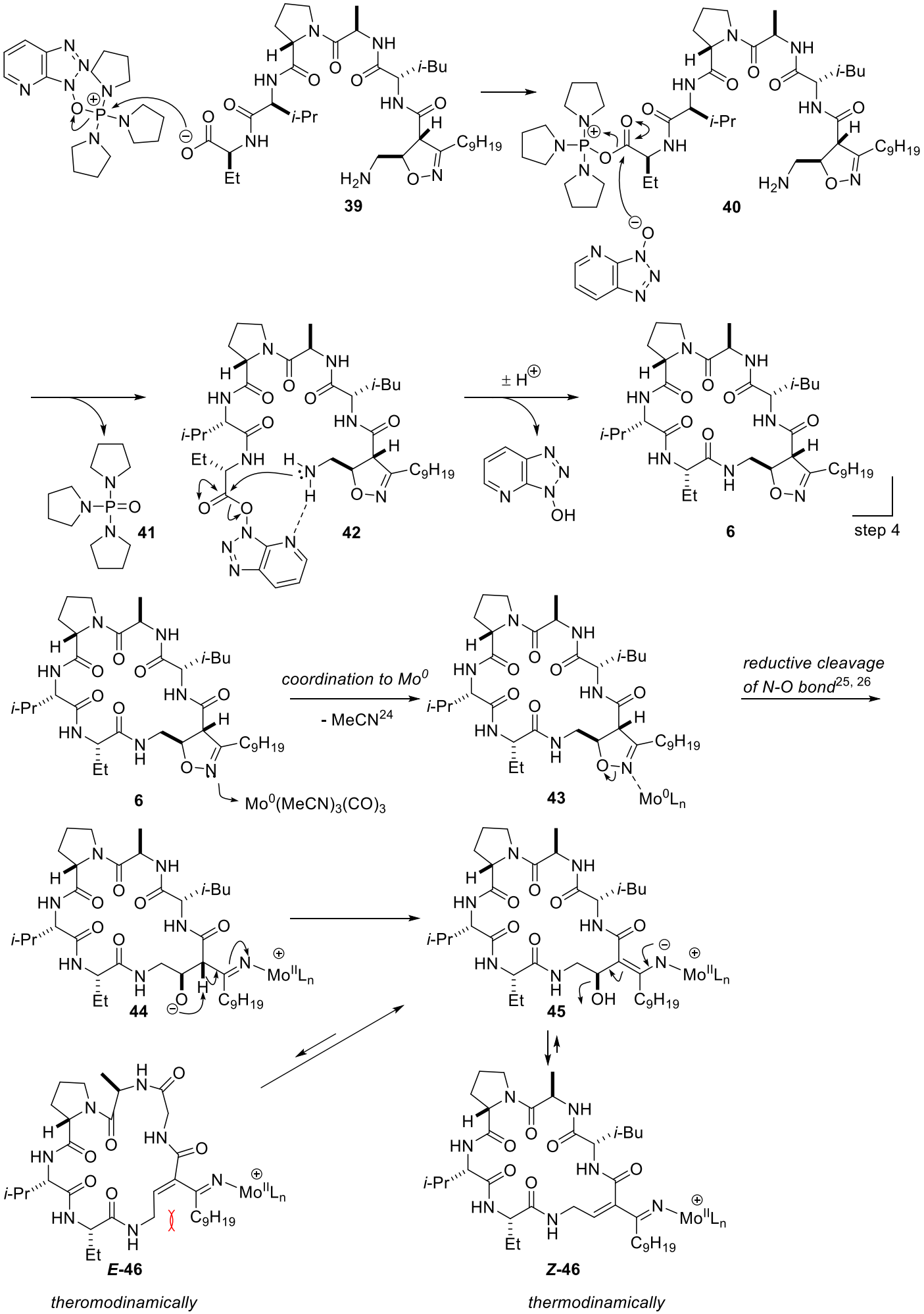
39
40
41
42
6
step 4
coordination to Mo0
- MeCN24
Mo0(MeCN)3(CO)3
43
reductive cleavage
of N-O bond25, 26
44
45
E-46
Z-46
theromodinamically
disfavored
thermodinamically
favored

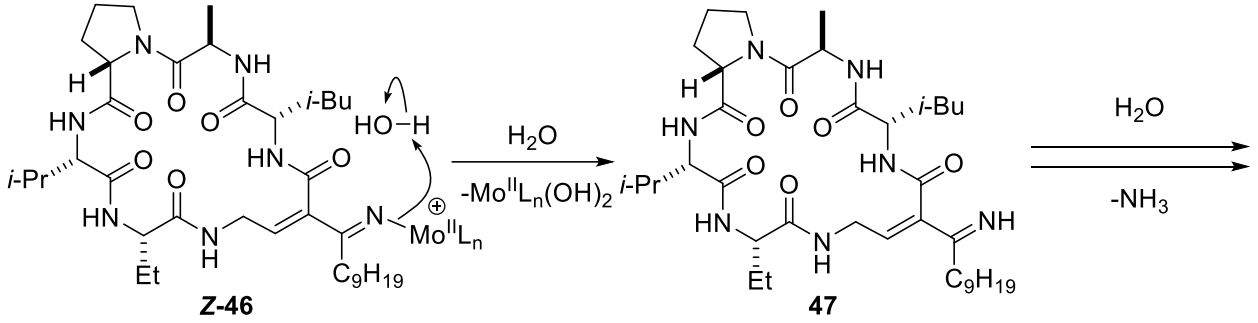
H2O
-Mo^IIL_n(OH)2
H2O
-NH3
Z-46
47

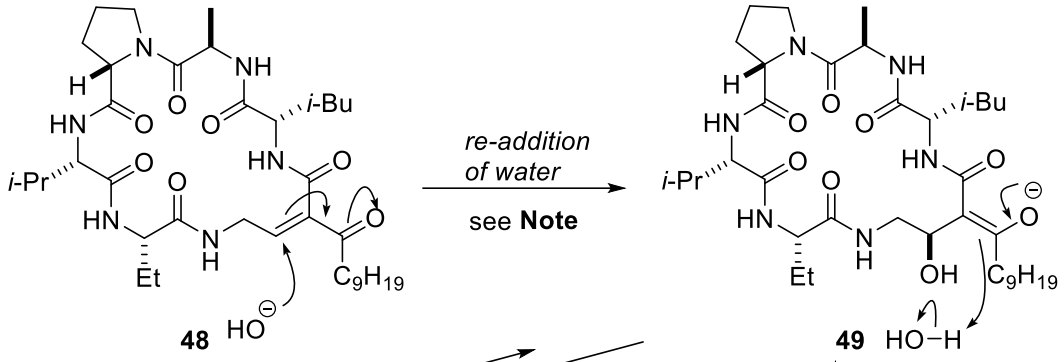
re-addition
of water
see Note
48
49

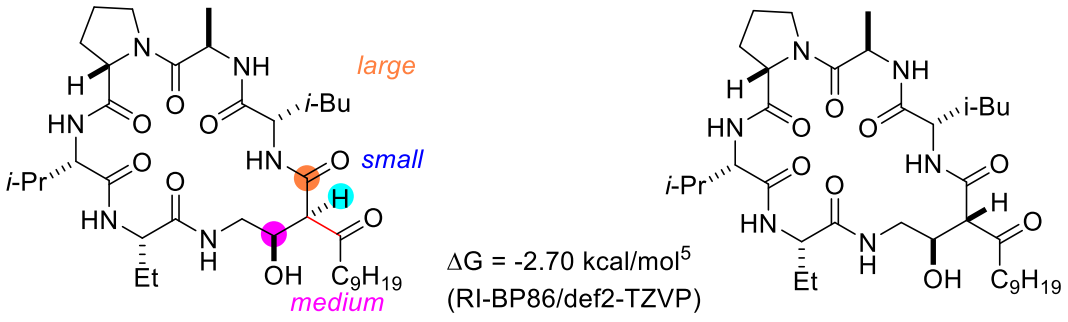
large
small
medium
ΔG = -2.70 kcal/mol5
(RI-BP86/def2-TZVP)
7
epi-7

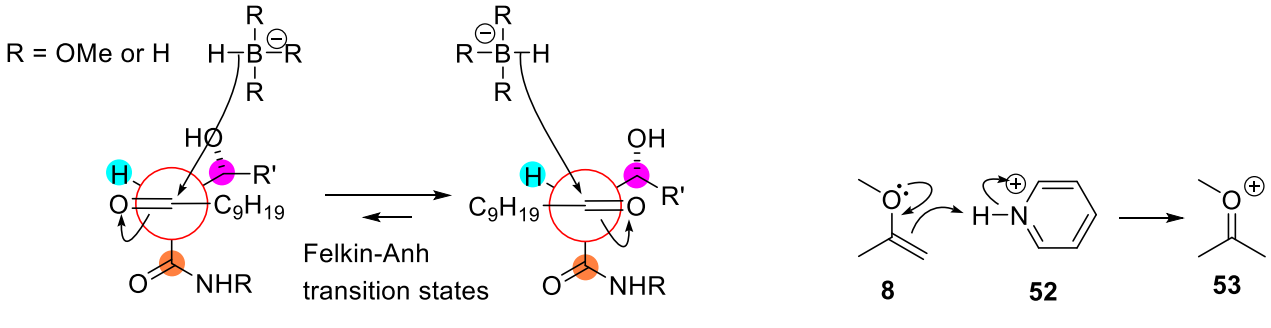
R = OMe or H
Felkin-Anh
transition states
7-1
7-2
8
52
53

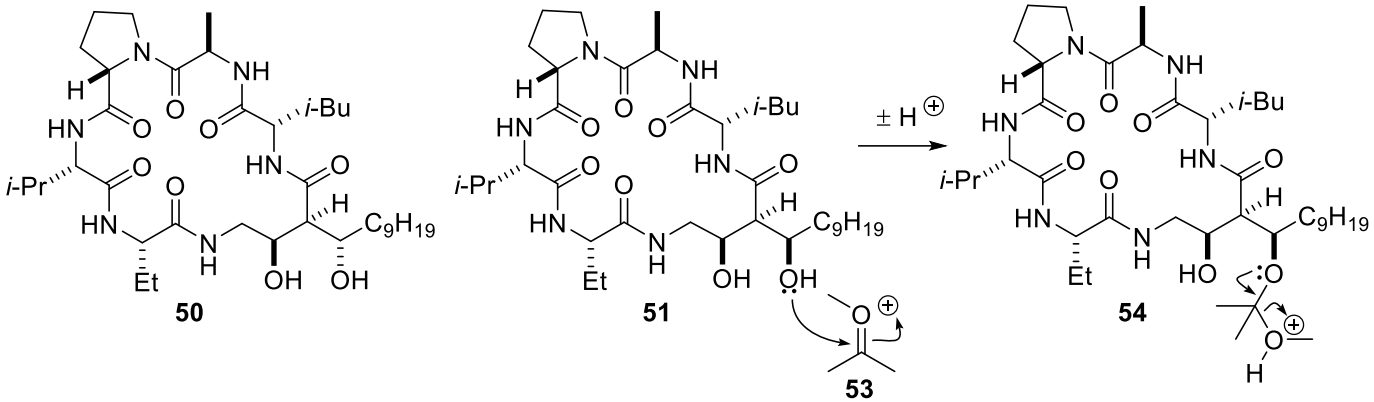
NaBH4-n(OMe)n
(0 ≤ n ≤ 3); workup
NaBH4-n(OMe)n
(0 ≤ n ≤ 3); workup
± H
50
51
53
54

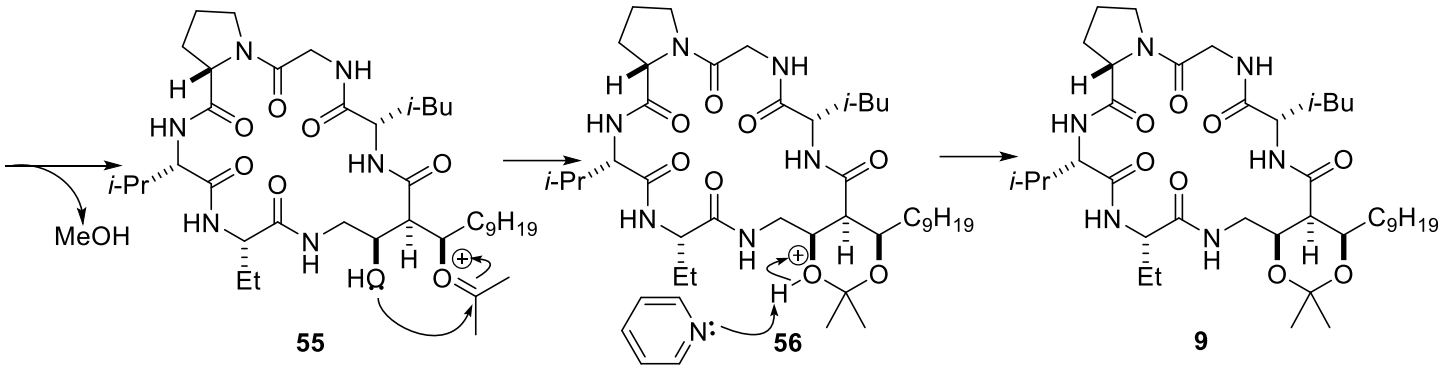

Note

C25(*R*)-configured **49** is presumably thermodynamically preferred to C25(*S*)-configured ***epi*-49** because C25 configuration **6'** of was not retained after treating with $Mo(MeCN)_3(CO)_3$[5].

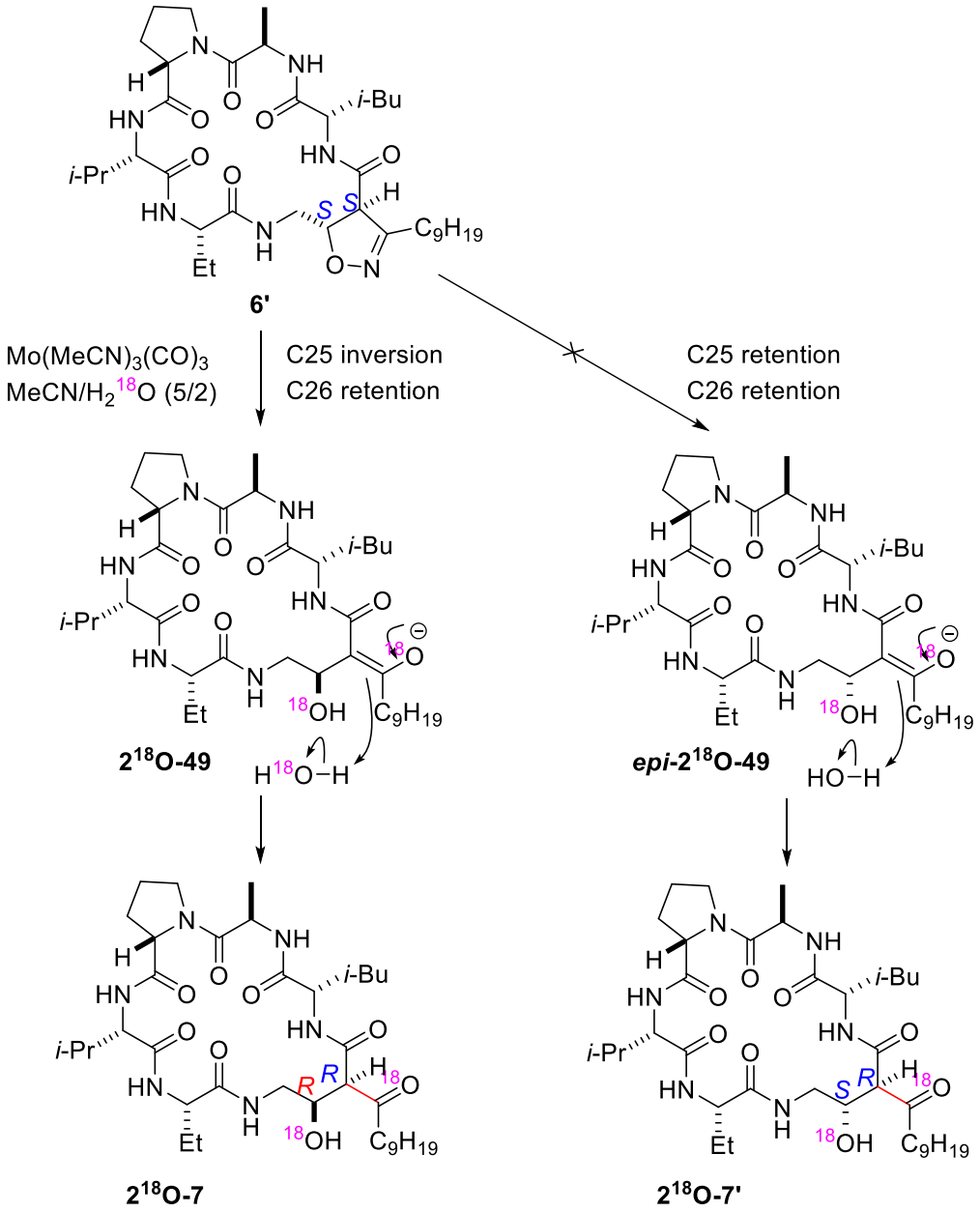

References

1. Thompson, D. S.; Carlisle, P. L.; Kadosh, D. *Eukaryot. Cell* **2011**, *10*, 1173.
2. Wu, C.; Cichewicz, R.; Li, Y.; Liu, J.; Roe, B.; Ferretti, J.; Merritt, J.; Qi, F. *Appl. Environ. Microbiol*. **2010**, *76*, 5815.
3. Joyner, P. M.; Liu, J.; Zhang, Z.; Merritt, J.; Qi, F.; Cichewicz, R. H. *Org. Biomol. Chem.* **2010**, *8*, 5486.
4. Wang, X.; Du, L.; You, J.; King, J. B.; Cichewicz, R. H. *Org. Biomol. Chem.* **2012**, *10*, 2044.
5. Pultar, F.; Hansen, M. E.; Wolfrum, S.; Böselt, L.; Fróis-Martins, R.; Bloch, S.; Kravina, A. G.; Pehlivanoglu, D.; Schäffer, C.; LeibundGut-Landmann, S.; Riniker, S.; Carreira, E. M. *J. Am. Chem. Soc.* **2021**, *143*, 10389.
6. Yoshida, Y.; Ukaji, Y.; Fujinami, S.; Inomata, K. *Chem. Lett.* **1998**, *27*, 1023.
7. Ukaji, Y.; Sada, K.; Inomata, K. *Chem. Lett.* **1993**, *22*, 1847.
8. Karplus, M. *J. Chem. Phys.***1959**, *30*, 11.
9. Karplus, M. *J. Am. Chem. Soc.* **1963**, *85*, 2870.
10. Haasnoot, C. A. G.; de Leeuw, F. A. A. M.; Altona, C. *Tetrahedron* **1980**, *36*, 2783.
11. Wang, A. C.; Bax, A. *J. Am. Chem. Soc.* **1996**, *118*, 2483.
12. Gutowsky, H. S.; Mochel, V. D.; Sommers, B. G. *J. Chem. Phys.* **1962**, *36*, 1153.
13. Williams, D. H.; Bhacca, N. S. *J. Am. Chem. Soc.* **1964**, 86, 2742.
14. Altona, C.; Francke, R.; de Haan, R.; Ippel, J. H.; Daalmans, G. J.; Westra Hoekzema, A. J. A.; van Wijk, J. *Magn. Reson. Chem.* **1994**, *32*, 670.
15. For a review, see Coxon, B. *Adv. Carbohydr. Chem. Biochem.* **2009**, *62*, 17.
16. Altona, C. Vicinal Coupling Constants and Conformation of Biomolecules. In *Encyclopedia of NMR*; Harris, R. K., Wasylishen, R. E., Eds.; John Wiley & Sons, Inc.: New York, 2012; pp 5364–5377.
17. $^{3}J_{H\text{-}H}$ can be instantly estimated in this URL: https://www.colby.edu/chemistry/NMR/scripts/altona/altona.html
18. Rychnovsky, S. D.; Skalitzky, D. J. *Tetrahedron Lett.* **1990**, *31*, 945.
19. Evans, D. A.; Rieger, D. L.; Gage, J. R. *Tetrahedron Lett.* **1990**, *31*, 7099.
20. Rychnovsky, S. D.; Powers, J. P.; Lepage, T. J. *J. Am. Chem. Soc.* **1992**, *114*, 8375.
21. Rychnovsky, S. D.; Rogers, B.; Yang, G. *J. Org. Chem*. **1993**, *58*, 3511.
22. Rychnovsky, S. D.; Yang, G.; Powers, P. *J. Org. Chem.* **1993**, *58*, 5251.
23. Guarna, A.; Guidi, A.; Goti, A.; Brandi, A.; De Sarlo, F. *Synthesis* **1989**, *1989*, 175.
24. Nitta, M.; Yi, A.; Kobayashi, T. *Bull. Chem. Soc. Jpn.* **1985**, *58*, 991.
25. Nitta, M.; Kobayashi, T. *J. Chem. Soc. Chem. Commun.* **1982**, 877.
26. Tranmer, K. T.; Tam, W. *Org. Lett.* **2002**, *4*, 4101.